PUBLICATION I

Enhanced Plastic Deformations of Nanofibrillated Cellulose Film by Adsorbed Moisture and Protein Mediated Interactions

Biomacromolecules, 2015, 16 (1), pp 311–318
DOI: 10.1021/bm501514w

BioMACROMOLECULES

Article

pubs.acs.org/Biomac

Enhanced Plastic Deformations of Nanofibrillated Cellulose Film by Adsorbed Moisture and Protein-Mediated Interactions

Jani-Markus Malho,*[,†] Claudiane Ouellet-Plamondon,[‡] Markus Rüggeberg,[§,∥] Päivi Laaksonen,[†,⊥] Olli Ikkala,[#] Ingo Burgert,[§,∥] and Markus B. Linder*[,†,○]

[†]VTT Technical Research Centre of Finland, Tietotie 2, P.O. Box 1000, FI-02044, Espoo, Finland

[‡]ETH-Zürich, Inst. Bau-u. Infrastrukturmanagement, Stefano-Franscini-Platz 5, 8093 Zürich, Switzerland

[§]ETH-Zürich, Institute for Building Materials (IfB), Stefano-Franscini-Platz 3, 8093 Zürich, Switzerland

[∥]Empa, Applied Wood Materials Laboratory, Überlandstrasse 129, 8600 Dübendorf, Switzerland

[⊥]Aalto University, Department of Materials Science, P.O. Box 16200, FI-00076 Aalto, Finland

[#]Aalto University, Department of Applied Physics, P.O. Box 15100, FI-00076 Aalto, Finland

[○]Aalto University, Department of Biotechnology and Chemical Technology, P.O. Box 16100, FI-00076 Aalto, Finland

Supporting Information

ABSTRACT: Biological composites are typically based on an adhesive matrix that interlocks rigid reinforcing elements in fiber composite or brick-and-mortar assemblies. In nature, the adhesive matrix is often made up of proteins, which are also interesting model systems, as they are unique among polymers in that we know how to engineer their structures with atomic detail and to select protein elements for specific interactions with other components. Here we studied how fusion proteins that consist of cellulose binding proteins linked to proteins that show a natural tendency to form multimer complexes act as an adhesive matrix in combination with nanofibrillated cellulose. We found that the fusion proteins are retained with the cellulose and that the proteins mainly affect the plastic yield behavior of the cellulose material as a function of water content. Interestingly, the proteins increased the moisture absorption of the composite, but the well-known plastifying effect of water was clearly decreased. The work helps to understand the functional basis of nanocellulose composites as materials and aims toward building model systems for molecular biomimetic materials.

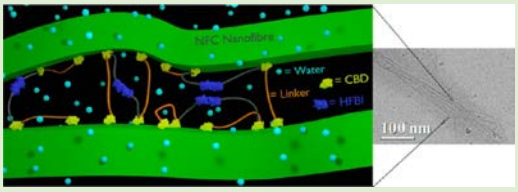

INTRODUCTION

Biological structural materials have inspired materials scientists to understand routes to combine high stiffness and strength with promoted toughness within a single material and, additionally, being sustainable and lightweight.[1,2] Classically, they seem to be conflicting properties, as stiffness and strength could be thought to need rigid and firmly interlocked reinforcing units, whereas toughness and suppressed catastrophic crack growth require ability to consume fracture energy using dissipative movements of the structural units.[3] Combining these requirements has turned out to be subtler than simply constructing composites or nanocomposites based on hard and soft domains.[4−6] Selected biological structural materials provide inspiration in this context, such as dragline silk, various shells, like nacre, and insect exoskeletons.[7] Silk is particularly instructive for the present case, as it is all-organic macromolecular system.[8,9] The reinforcing units are a few nanometers thick protein β-sheets as connected by more flexible protein domains consisting of folds that can efficiently consume mechanical deformation energy, involving sacrificial bonds and loopings that form hidden lengths.[10,11] To achieve the feasible combination of mechanical properties, the different mechanisms work in synergy in parallel and balanced ways.

In synthetic materials, progress has been made, inspired by biological structural materials.[7,12−14] Tough inorganic/organic layered biomimetic composites have been produced by ice-templating and also using sequential spin coatings.[15,16] One-step self-assemblies of core−shell colloidal polymer-coated sheets have been shown to possess high strength and stiffness as well as stable crack growth under wet conditions.[4,17] Graphene has also been incorporated as the reinforcing unit by physical exfoliation into a native nanofibrillated cellulose matrix with improved ultimate tensile strength, stiffness, and toughness.[18]

Nanofibrillated cellulose (NFC) is nanofibrils with a high aspect ratio being typically a few micrometers in length and 5−20 nm in width possessing exceptional mechanical properties with high modulus of about 140 GPa and tensile strength even in the GPa range.[19,20] The cellulose nanofibrils play a key role

Received: October 13, 2014
Revised: November 22, 2014
Published: November 24, 2014

in the mechanical properties of plant cell walls, and their interplay with matrix polymers like hemicellulose, lignin, or pectin dictates the performance of the natural composites.[21,22] Being highly abundant and renewable, NFC is an interesting option for nanocomposites.[23] NFC is obtained by grinding and fluidization of, for example, pulp in combination with different pretreatments.[24−27] The interfibrillar interactions (mostly hydrogen bonds but also other weak interactions) are expected to dominate the behavior and structure of an unmodified native NFC film (nanopaper),[23] making it mechanically strong. Although the energy dissipation under mechanical loading can be high, the tightly packed random network structure shows typically brittle failure as cracks grow catastrophically upon deformation. One could speculate that this is due to the inability of the rigid colloidal level NFC fibrils to undergo dissipative relative movements to further consume mechanical energy. A trivial approach would be to expose the films to humidity, where the adsorbed water could plasticize the film. A more versatile approach could be to tune the interactions of the NFC by constructing different polymeric shells around the NFC cores.[28] So far, for several such approaches, the stress−strain curves in tensile measurements have been remarkably similar, with an initial elastic part and then a smooth yield-point manifested as a slope change and followed by plastic strain-stiffening. One report that deviates from this NFC performance pattern describes the introduction of surface modifications to introduce sacrificial bonds in cellulose nanocrystals, where the sacrificial bonds were based on acrylate polymer brushes, incorporating supramolecular ureidine pyrimidone groups and resulted in noncatastrophic crack propagation and substantial yielding by necking in tensile deformation.[29] In all above cases, the nanocellulose-based films and composites were prepared from solvent-dispersed phase upon solvent removal, which leads to jamming into highly packed solid phase with reduced dynamics. This phase can be regarded as colloidal glass. Deformations and colloidal dynamics of rod-like colloidal glasses are not yet fully understood.[30−32]

The above-mentioned arguments suggest in general pursuing toward finding protocols to tune the deformation characteristics of nanocellulose-based colloidal glasses by involving side chains with supramolecular binding units. Our hypothesis here was that proteins are, par excellence, macromolecules allowing supramolecular interactions based on tunable and specific protein folding-based interactions, as well as enabling non-specific hydrogen bonds. Here we selected a bifunctional fusion protein to decorate NFCs, consisting of groups allowing binding on NFC and a group that allows supramolecular binding to other similar groups. The supramolecular motif was selected to be class II hydrophobin (HFBI), which is known to have a high intermolecular binding constant. As the second motif we selected cellulose-binding domains, denoted here DCBD, where two CBDs were included due to their small size to allow a balanced structure with HFBI. The two types of motifs are connected by a linker. Therefore, the genetically produced "diblock protein" is here denoted as DCBD-HFBI.[33] Both HFBI and CBDs are found in nature, wherein HFBI is known to self-assemble on (hydrophobic) interfaces in aqueous environments[34] and the CBDs to have a high affinity to cellulose surfaces.[35] The behavior of DCBD-HFBI has earlier been studied within an NFC matrix[36] and utilized to exfoliate multilayered graphene in aqueous environment.[37] Furthermore, the same approach has been taken even further to mimic the structure of nacre[1] by combining native NFC fibrils, multi-layered graphene, and DCBD-HFBI in an aqueous environment via self-assembly, where the DCBD-HFBI was used as a glue to bind hydrophobic graphene flakes together with NFC fibrils.[38]

Here we study how the DCBD-HFBI functions within unmodified native NFC matrix to gain insights on the characteristics of the plastic deformation behavior. The initial amount of DCBD-HFBI in relation to the NFC was chosen to be high to saturate the binding on the NFC fibrils surfaces,[36] while the sample preparation should remove the unbound proteins from the film. To better understand interactions generated by the proteins and the NFC fibrils within a freestanding film, the effect of the degree of hydration on the mechanical behavior of unmodified NFC film and the NFC/DCBD-HFBI hybrid films is studied. Hydration is known to have major effects on the interactions of biomaterials and on the performance of composites.[17,39] More importantly, moisture is an inevitable part of materials in most of the systems highlighting the importance of understanding the role of water molecules within the system.

MATERIALS AND METHODS

Materials. NFC was processed by mechanical disintegration of bleached birch kraft pulp by 10 passes through a M7115 Fluidizer (Microfluidics Corp.), essentially according to previous reports.[26] The solid content of the prepared water dispersion was 1.9%. The bifunctional fusion protein consisted of one hydrophobin part linked to two different CBDs in series. The HFBI-hydrophobin from *Trichoderma reesei*[34] was used and the two CBDs were from the enzymes Cel7A (previously CBHI)[40] and Cel6A (previously CBHII),[41] also from *T. reesei*. These modules of the proteins were connected by polypeptide linker regions, as previously reported.[33] The abbreviation DCBD-HFBI is used for the fusion protein. The fusion protein was produced by recombinant means in *T. reesei* and purified by aqueous two-phase extraction, as described previously.[33] The protein was then purified by preparative reversed phase high performance liquid chromatography (RP-HPLC) using a water acetonitrile gradient with 0.1% trifluoroacetic acid. The identity and concentration were verified by amino acid analysis. Mass spectroscopy was additionally used to verify the identity. The proteins were lyophilized after purification.

Film Preparation. NFC dispersions were diluted in Milli-Q water (mQ) so that the concentration was 4.0 gL^{-1} based on the weight mass of the NFC batch. DCBD-HFBI was weighted in a plastic tube and diluted in mQ to concentration of 4.0 gL^{-1}. The NFC and DCBD-HFBI were mixed so that both NFC and DCBD-HFBI had the concentration of 2.0 gL^{-1} (108 μM) in the final volume of 2.4 mL. With these starting conditions it is calculated using that at equilibrium the bound amount is 19 μmol/g and the free concentration is 69 μM (K_d= 2.4 μM, B_{max} 20 μmol/g, M_w = 18436 g/mol).[36] Before vacuum filtration, the dispersions were sonicated by 2000 J per 2.4 mL dispersion via tip sonicator (Vibra-Cell VCX 750, Sonics and Materials Inc.) to enhance the dispersity of the fibrils and NFC/DCBD-HFBI mixtures. The used power was 40% of the full output power. The dispersions were vacuum filtrated using Durapore membranes (GVWP, 0.22 μm, Millipore, U.S.A.) and an O-ring to determine the diameter of the films. A press with a 300 g load for 10 min was applied to prevent wrinkling. At the end, the films were dried overnight in an oven at +60 °C.

Relative Humidity Control. The microtensile tests at 85% and 50% relative humidity (RH) were conducted in a controlled desiccator monitored with a hygrometer Testo 608-H1. At 85% RH, samples were conditioned in a controlled humidity room until the test time. The relative humidity of the desiccator was achieved by a homemade system of flowing air heated and humidified by boiling water on a hot plate. Potassium chloride contributed to maintain the relative humidity of the desiccator. For the drier conditions (25%RH and 5%RH),

samples were dried in the oven at 60 °C and conditioned in a desiccator equipped with a compressed air line. The relative humidity control was achieved by varying the pressure delivered to the desiccator from 0 to 1 bar with potassium acetate.

Scanning Electron Microscopy. The thickness of the films was measured with a scanning electron microscope (SEM) FEI Quanta 200F (U.S.A.), both in low and high vacuum conditions. A thin Au layer was sputtered on the samples in high vacuum.

Tensile Testing. Tensile test were conducted using a microtensile testing device. A detailed description of this device can be found in Burgert et al.[42] The high precision linear stage was an Owis Limes 60 featuring a two-phase step motor. The controller was a PI micos Pollux type 1. Tensile tests were carried out using a 50 N load cell with a nominal strain rate of 8 $\mu m \cdot s^{-1}$. The gauge length was set to 10 mm for all of the samples. At least four specimens were measured from each sample. Sample sizes were 2.0 cm × 2.0 mm × 8−14 μm, length, width, and thickness, respectively. Sample thicknesses were measured using SEM. Here, at least six measurements from a cross-section of a sample were measured to calculate average value for thickness. The widths were measured with a digital slide gauge (Digimatic, Mitutoyo). The mechanical tensile tester was placed inside desiccator during the measurements, so the measurements could be done in a controlled humidity. Depending on the desired relative humidity, dry air or humid air was pumped into the desiccator. For the measurements at 50%RH and 85%RH samples were first stored overnight in humidity controlled rooms. Before testing they were moved to the humidity controlled desiccator. Samples that were measured at 5%RH were taken directly from the oven to the dry desiccator and tested. Samples measured at 25%RH were taken from oven and equilibrated to 25% RH in a desiccator prior to testing.

FT-IR Spectroscopy. The FT-IR spectroscopy measurements were performed using a PerkinElmer Spectrum 100 in the 4000 to 600 cm^{-1} range with a resolution of 4 cm^{-1}. The resulting spectra represent averages of 50 scans. They were baseline-corrected for CO_2 and water.

Dynamic Vapor Sorption (DVS). Moisture sorption and desorption isotherms of one unmodified NFC film and one NFC/DCBD-HFBI film were generated with a VTI-SA Vapor Sorption Analyzer (TA Instruments). Measurements were performed at 10, 25, 50, and 85% relative humidity. The samples were initially dried at 105 °C for 60 min. Equilibrium was assumed when there was no mass change more than 0.0010% in 2 min with the condition that equilibrium must be reached within 300 min.

TGA. The thermogravimetric analysis was conducted with a TGA Q50 (TA Instruments). A 2.2 mg sample was placed in a platinum pan and heated 10 °C/min until 1000 °C in a nitrogen current. The thermogravimetric (TG) curves express the percent mass loss as a function of temperature and the derivative TG show the mass loss rate as a function of temperature.

RESULTS AND DISCUSSION

The structural and chemical composition of the NFC/DCBD-HFBI composites was qualitatively evidenced with FTIR and TGA. First, FTIR spectra of the NFC/DCBD-HFBI films show two additional bands in comparison to the spectra of the pure NFC films which confirm the presence of protein in the modified films. One band at 1639 cm^{-1} represents an amide I band of protein associated with the C═O vibration in antiparallel β-sheets,[43] and the other band at 1518 cm^{-1} corresponds to an amide II band associated with the N−H bending vibration and the C−N stretching vibration (see the Supporting Information, Figure S1). Second, the TGA of the NFC/DCBD-HFBI film showed a pronounced shoulder in the spectrum, which corresponds to the degradation of the protein (see Supporting Information, Figure S2). Films containing protein were approximately 20−40% thicker than controls not containing protein, indicating a 70−80% volume fraction of NFC in the protein-containing films.

Furthermore, the water vapor absorption−desorption properties of an unmodified NFC and NFC/DCBD-HFBI films were different. The masses of films were determined upon exposure to different relative humidity conditions and the water uptake was evaluated (Figure 1). The results show that NFC/DCBD-HFBI films adsorbed more moisture than unmodified NFC films over the entire range of humidity from 5 to 85% RH. Especially at high humidity levels, the differences between the two films were significant. In addition, the TGA measurements displayed higher amount of evaporated moisture for the NFC/DCBD-HFBI film (see Supporting Information, Table 1).

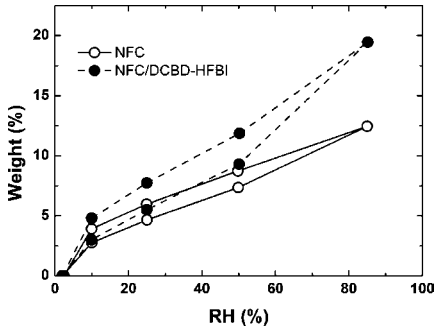

Figure 1. Water vapor adsorption−desorption isotherms of unmodified NFC and NFC/DCBD-HFBI films. The *y*-axis shows relative change.

Tensile testing of both unmodified NFC film and protein-containing NFC/DCBD-HFBI film were performed at four different humidities: 5%RH, 25%RH, 50%RH, and 85%RH. In Figure 2, representative stress−strain curves are shown. The average values for calculated parameters are shown in Figure 3. In all cases, the shape of the stress−strain curves consisted of an initial elastic part, then a yield point where the slope changed, and following that, a plastic region at high strains that showed strain stiffening.

Figure 2a shows the effect of humidity on the tensile properties of unmodified NFC film. At 5%RH, the maximum stress was near 250 MPa, whereas the strain-to-failure was relatively small (5.5%). We found that, upon increasing moisture content, the yield point became more distinct at approximately the same strain values, and that the yield stress became substantially reduced in humid samples. Notably the plastic strain region was considerably increased. For 85%RH, the strain was relatively high (17%) as was the ultimate stress (200 MPa). As a general trend, the Young's moduli decreased with absorbed humidity. A pronounced effect of humidity was seen in the plastic region, where the slope of the stress−strain curve was significantly reduced upon increased moisture (see Figure 5). The values for the slopes were calculated directly after the yield points. This signifies the plasticizing effect of water to allow dissipative mutual sliding of the NFC fibrils. The dissipation was further investigated using cyclic mechanical testing in the plastic region (Figure 4) showing that the elongation does not recover after the yield-point. Finally, we remark that upon tearing both the protein containing and the unmodified NFC films qualitatively showed catastrophic crack propagation at all humidity levels.

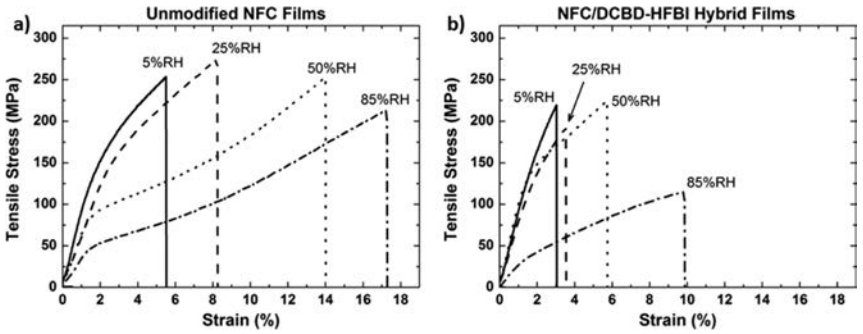

Figure 2. Representative stress−strain curves for (a) unmodified NFC and (b) NFC/DCBD-HFBI hybrid films in four different humidities. Solid lines represent measurements at 5%RH, dashed lines at 25%RH, dotted lines at 50%RH, and dash dotted lines at 85%RH.

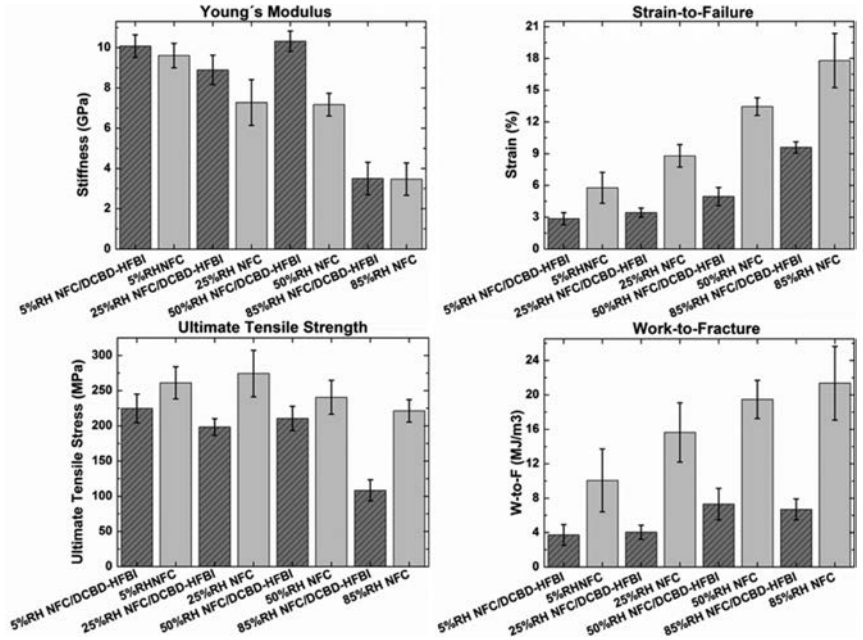

Figure 3. Young's modulus, strain-to-failure, ultimate tensile strength, and work-to-fracture of the noncyclic measurements for the unmodified NFC films and the NFC/DCBD-HFBI hybrid films at four different humidities with standard deviation. The values for unmodified NFC film are shown with gray bars and the values for the NFC/DCBD-HFBI hybrid film in dark gray lined columns.

Both quantitatively and qualitatively there were significant differences in the stress−strain curves of NFC/DCBD-HFBI and unmodified NFC films, see Figure 2. At all humidity levels, the strain values for NFC/DCBD-HFBI were less than those of unmodified NFC, and notably at 85%RH, the ultimate strength was only half of that of unmodified NFC. In the plastic zone, the initial slope in the plastic region increased particularly strongly upon reduced water content, Figure 5b,d.

The same data show that the plastifying effect of water is lower in the protein-containing films than in those without proteins. This is in interesting contrast to the observation that the protein-containing samples actually adsorbed more water in the sorption measurements (Figure 1). The slopes of the stress−strain curves in the plastic region for films with and without protein showed the largest relative difference around 50% RH, being double at this range (Figure 5b,d). The plastifying effect of water is interpreted in terms of water molecules competing with interfibril hydrogen bonding, which allows fibrils to slip more easily past each other. The presence of protein molecules leads to a situation where more water can be accommodated in the structure, but the effect of water as a plasticizer is decreased. This apparent contradiction may be explained by considering the natural environment of proteins. Proteins naturally function in aqueous environments but rely on hydrogen bonding for interactions. To do so, they rely on precise structures, which are able to form multivalent, mutually strengthening, synergistic bonding. At the same time, they offer many hydration sites around their structures. Therefore, the

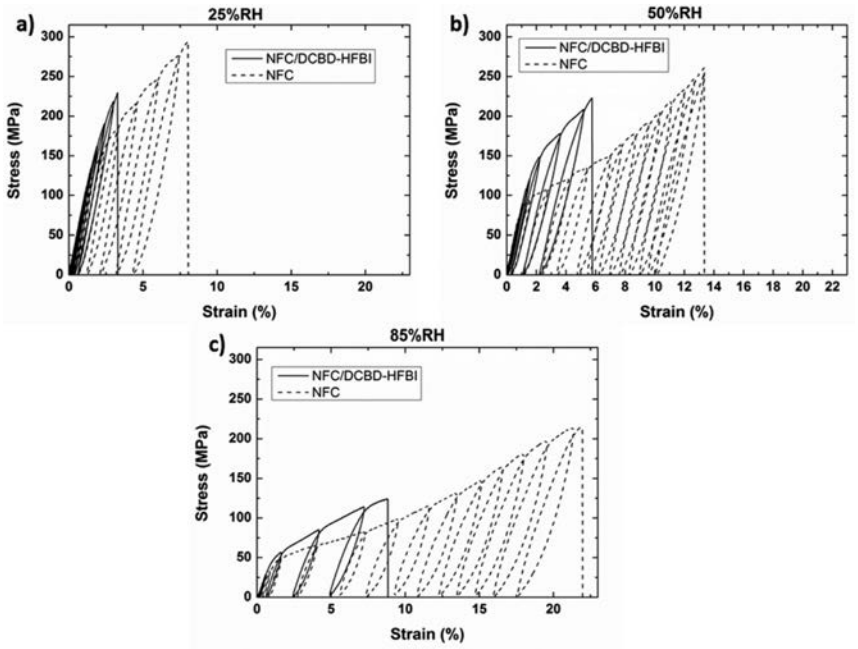

Figure 4. Representative stress–strain curves of the unmodified NFC (drawn as dashed black line) and NFC/DCBD-HFBI films (solid black line) from cyclic tensile tests measured at 25%RH, 50%RH, and 85%RH (a–c, respectively).

ability of the protein-containing films to both absorb more water and simultaneously resist the plasticizing effect may be a logical consequence of the natural structure and function of the embedded proteins.

Since the protein matrix affected the material mainly through interaction during plastic deformation, while the effect was relatively minor for the elastic modulus the results suggest that we only partly can rationalize results through a model where the protein would act as an adhesive matrix between fibrils. First, we conclude that there is a clear effect of proteins as an adhesive element based on the arguments presented above. However, since the elastic modulus remained mostly unaffected by the protein addition we hypothesize that the initial elastic stiffness of the structures is dominated by other interactions. A likely reason is the entanglement of the long NFC fibrils, and involving bonding not immediately affected by the protein, that is, a situation where in a velcro-like manner hooks and loops are entangled. Such mechanical interlocking and entanglement is expected because of the very long aspect ratios found in NFC fibrils. Only when the strain leads to irreversible transformations in the entangled structures, that is, during plastic deformation, do we note a role of the protein. This suggests that in protein containing samples the rearrangements lead to increased interactions between fibrils over higher length scales. The relatively large dimensions of the protein perhaps allow a more efficient spanning of the space in between the fibrils. A plausible mechanism for linkage is suggested in Figure 6. According to this model, the CBD-parts adhere to the cellulose and interchain linkage is mediated by HFBI-multimerization interactions or by bridges formed by the linker between cellulose binding domains. The latter case may be less favorable since we know that the linkage of CBD-domains leads to a higher affinity in binding. The reason for this increase in affinity lies in the lower entropy cost for the binding of the second domain once the first one has bound. This reduction in entropy cost is expected to be more beneficial if binding sites were close to each other, that is, on the same fibril rather than separated on different fibrils. During the later stages of plastic deformation, the protein containing material shows less ultimate stress compared to the nonprotein controls. It is also noted that during plastic deformation the samples without protein showed a characteristic concave-up shape of the stress–strain curve. This is indicative of a strain-stiffening due to reorganization and sliding of fibrils relative to each other. The effect is seen in both static and cyclic testing. This effect is not observed in the protein-containing samples. We can interpret this effect in terms of a resistance to plastic deformation caused by the protein. Because this increased resistance to deformation also leads to less stress-relieving rearrangements, it is also logical that the ultimate strength of the protein containing samples is somewhat decreased. This is because the protein apparently does not allow sliding of fibrils to relieve local stress concentration, and therefore lead to higher local concentrations of stress and subsequent rupture of fibrils.

As a note, however, we see that for the samples measured at 50% RH the protein containing films show a pronounced stiffness. At this humidity there is also a clearly elevated yield point, indicating some sort of increased molecular interaction between fibrils. This is an interesting observation that somewhat deviates from the overall trends observed in the samples and for which the significance is not clear. It may be

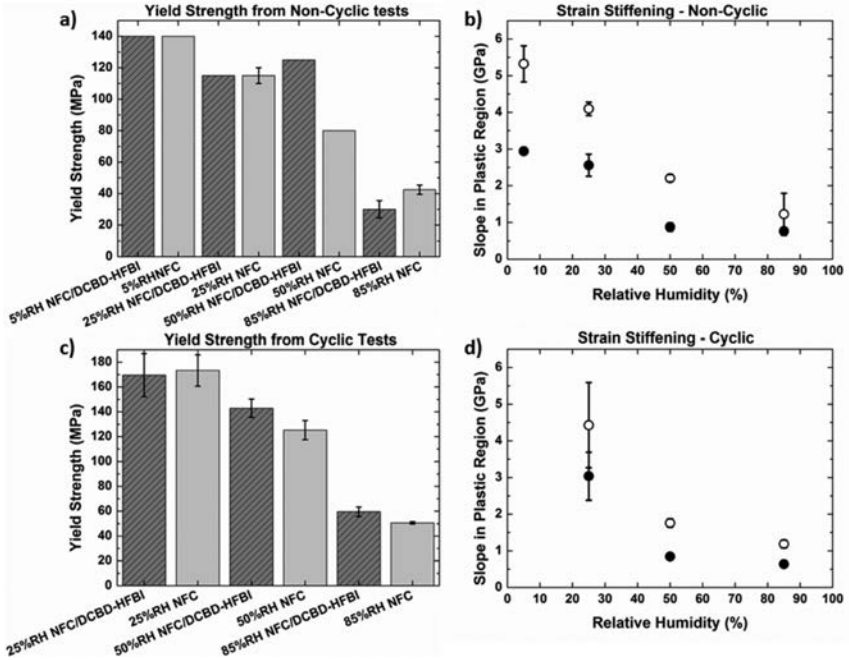

Figure 5. Average yield stress values from (a) noncyclic measurements and (c) cyclic measurements for unmodified NFC and NFC/DCBD-HFBI films in four different humidities. (b) The calculated slope in the plastic region from noncyclic measurements after the yield point at 5%RH, 25%RH, 50%RH, and 85%RH, respectively, as a function of relative humidity, where unmodified NFC film is drawn with black round dots and the NFC/DCBD-HFBI hybrid film with hollow black round circles. (d) The slope in the plastic region at 25%RH, 50%RH, and 85%RH, respectively, as a function of relative humidity in the cyclic measurements, where unmodified NFC film is drawn with filled round circles and the NFC/DCBD-HFBI hybrid film with nonfilled black circles. All results are shown with standard deviation.

that, at this particular humidity, there is an optimal resistance of protein containing samples for the plastifying effect of water.

Qualitatively, the present stress−strain curves resemble those of several glassy polymers. It is interesting to contemplate the differences between polymeric molecular glasses and nanofibrillar colloidal glasses. In polymeric glasses, the initial part at low strains is elastic, allowing complete recovery of the initial structure after removing the deformation forces. After the yield point, the deformation starts to be nonaffine, where the polymeric chains start sliding past each other, thus, consuming energy. In the process, the material starts to be slightly anisotropic. Strain stiffening is more pronounced for long polymers, obviously as under deformation the chains become slightly stretched due to larger number of entanglements in longer polymers. The strain stiffening is an activated process, where the strain stiffening is higher at high strains and becomes smaller upon increased temperature, obviously as the chains can slide more easily past each other's at higher temperatures, with higher free volume. It has been hypothesized that in polymeric glasses, large strain stiffening is connected to reduced strain location and can lead to promoted toughness.[44] In polymeric glasses, there are still segmental dynamics, after the main dynamics has been arrested in glass transition. In rod-like colloidal glasses, one could expect similarities but also differences. The colloidal units obviously have more defined geometrical shapes, and therefore the packing reasons leading to arrested dynamics may be more pronounced and the secondary relaxations more suppressed. An important difference between the polymeric glasses and the present colloidal glasses is the aspect ratio, which in the NFC-based colloidal glasses is substantially smaller. This may require well-balanced supramolecular interactions between the NFC fibrils, which still remains a challenge for future work.

CONCLUSIONS

This work aims to control fracture energy dissipation in NFC-based films by using bifunctional genetically prepared fusion proteins, providing adsorption on NFC (cellulose binding domain, CBD) and supramolecular binding between the proteins (hydrophobin, HFBI). DCBD-HFBI fusion protein affects the properties of nanocellulose films. The resulting nanocellulose/protein colloidal glasses show a distinct yielding and a steeper slope in the plastic region. Still, toughness in the form of suppressed catastrophic crack growth could not be achieved. Increased water content caused easier sliding of fibrils in NFC-films, that is, water plasticized the films. Proteins in the films lead to an increased uptake of water but also resulted in a reduction of the amount of water that was available for sliding of fibrils. This study supports a central role of proteins in adhesive matrix functions in natural composites, but also suggests that the material properties are highly dependent on balanced structural arrangements at all length scales.

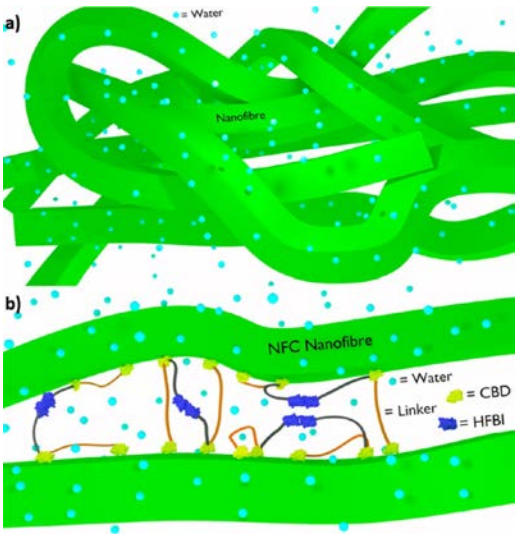

Figure 6. Schematic illustrations of (a) a highly entangled NFC fibrils matrix and (b) of the possible molecular structures of the NFC/DCBD-HFBI hybrid film. The most probable structure that would result in the modified mechanical performance is that the HFBI domains bind to each other while both of the CBDs in a DCBD-HFBI molecule would bind to the same NFC fibril causing molecular cross-linking of the NFC network. Another possibility is that the hydrophobins are bound to each other as in the first scenario, but the CBD domains bind separate NFC fibrils, where molecular cross-linking of the NFC fibrils would occur through CBDs and the HFBI domains. Both scenarios are possible and may take place at the same time, although cross-linking through a DCBD domains seems more unlikely based on previous studies.[35] Water molecules are highlighted with light blue dots. Hemicellulose is not included to the image due to the fact that no reliable information on the location of hemicelluloses is known to our understanding; furthermore both films contain the same amount of hemicellulose since the same batch of NFC was used for this study. Based on the mechanical tensile testing water molecules seem to be able to penetrate both unmodified NFC film and the NFC/DCBD-HFBI hybrid film affecting the mechanical performances. However, the DCBD-HFBI is likely to be able to outcompete the water molecules within the matrix, which is seen in the altered hydration dependent mechanical behavior.

■ ASSOCIATED CONTENT

Supporting Information

FT-IR spectra, cyclic tensile test results, and TGA data. This material is available free of charge via the Internet at http://pubs.acs.org.

■ AUTHOR INFORMATION

Corresponding Authors

*E-mail: jani-markus.malho@vtt.fi.
*E-mail: markus.linder@aalto.fi.

Notes

The authors declare no competing financial interest.

■ ACKNOWLEDGMENTS

The Scientific Center for Optical and Electron Microscopy (ScopeM) at ETH Zürich is acknowledged for the SEM images. Tekes (Naseva), VTT and the Academy of Finland (264493) are thanked for the financial support. This work was performed within centre of excellence in Molecular Engineering of Biosynthetic Hybrid Materials (hyber.aalto.fi). Emil Aaltonen Foundation, FinCEAL, and Bioregs graduate school are thanked for financial support. Riitta Suihkonen is thanked for purification of the proteins. I.B. thanks the Bundesamt für Umwelt and Lignum, Switzerland, for financial support of the Wood Materials Science group.

■ REFERENCES

(1) Espinosa, H. D.; Rim, J. E.; Barthelat, F.; Buehler, M. J. Merger of structure and material in nacre and bone: perspectives on de novo biomimetic materials. *Prog. Mater. Sci.* **2009**, *54*, 1059−1100.
(2) Weiner, S.; Addadi, L. Design strategies in mineralized biological materials. *J. Mater. Chem.* **1997**, *7*, 689−702.
(3) Song, F.; Soh, A.; Bai, Y. Structural and mechanical properties of the organic matrix layers of nacre. *Biomaterials* **2003**, *24*, 3623−3631.
(4) Walther, A.; Bjurhager, I.; Malho, J.-M.; Pere, J.; Ruokolainen, J.; Berglund, L. A.; Ikkala, O. Large-area, lightweight and thick biomimetic composites with superior material properties via fast, economic, and green pathways. *Nano Lett.* **2010**, *10*, 2742−2748.
(5) Rosilo, H.; Kontturi, E.; Seitsonen, J.; Kolehmainen, E.; Ikkala, O. Transition to reinforced state by percolating domains of intercalated brush-modified cellulose nanocrystals and poly(butadiene) in cross-linked composites based on thiol−ene click chemistry. *Biomacromolecules* **2013**, *14*, 1547−1554.
(6) Tang, Z.; Kotov, N. A.; Magonov, S.; Ozturk, B. Nanostructured artificial nacre. *Nat. Mater.* **2003**, *2*, 413−418.
(7) Meyers, M. A.; Chen, P.-Y.; Lin, A. Y.-M.; Seki, Y. Biological materials: structure and mechanical properties. *Prog. Mater. Sci.* **2008**, *53*, 1−206.
(8) Hardy, J.; Scheibel, T. Silk-inspired polymers and proteins. *Biochem. Soc. Trans.* **2009**, *37*, 677−681.
(9) Nova, A.; Keten, S.; Pugno, N. M.; Redaelli, A.; Buehler, M. J. Molecular and nanostructural mechanisms of deformation, strength and toughness of spider silk fibrils. *Nano Lett.* **2010**, *10*, 2626−2634.
(10) Keten, S.; Xu, Z.; Ihle, B.; Buehler, M. J. Nanoconfinement controls stiffness, strength and mechanical toughness of beta-sheet crystals in silk. *Nat. Mater.* **2010**, *9*, 359−367.
(11) Keten, S.; Buehler, M. J. Nanostructure and molecular mechanics of spider dragline silk protein assemblies. *J. R. Soc., Interface* **2010**, *7*, 1709−1721.
(12) Buehler, M. J. Turning weakness to strength. *Nano Today* **2010**, *5*, 379−383.
(13) Dunlop, J. W.; Weinkamer, R.; Fratzl, P. Artful interfaces within biological materials. *Mater. Today* **2011**, *14*, 70−78.
(14) Meyers, M. A.; McKittrick, J.; Chen, P.-Y. Structural biological materials: critical mechanics-materials connections. *Science* **2013**, *339*, 773−779.
(15) Bonderer, L. J.; Studart, A. R.; Gauckler, L. J. Bioinspired design and assembly of platelet reinforced polymer films. *Science* **2008**, *319*, 1069−1073.
(16) Munch, E.; Launey, M. E.; Alsem, D. H.; Saiz, E.; Tomsia, A. P.; Ritchie, R. O. Tough, bioinspired hybrid materials. *Science* **2008**, *322*, 1516−1520.
(17) Verho, T.; Karesoja, M.; Das, P.; Martikainen, L.; Lund, R.; Alegría, A.; Walther, A.; Ikkala, O. Hydration and dynamic state of nanoconfined polymer layers govern toughness in nacre-mimetic nanocomposites. *Adv. Mater.* **2013**, *25*, 5055−5059.
(18) Malho, J. M.; Laaksonen, P.; Walther, A.; Ikkala, O.; Linder, M. B. Facile method for stiff, tough, and strong nanocomposites by direct exfoliation of multilayered graphene into native nanocellulose matrix. *Biomacromolecules* **2012**, *13*, 1093−1099.
(19) Eichhorn, S.; Dufresne, A.; Aranguren, M.; Marcovich, N.; Capadona, J.; Rowan, S.; Weder, C.; Thielemans, W.; Roman, M.; Renneckar, S. Review: current international research into cellulose nanofibres and nanocomposites. *J. Mater. Sci.* **2010**, *45*, 1−33.

(20) Iwamoto, S.; Kai, W.; Isogai, A.; Iwata, T. Elastic modulus of single cellulose microfibrils from tunicate measured by atomic force microscopy. *Biomacromolecules* **2009**, *10*, 2571−2576.
(21) Keckes, J.; Burgert, I.; Frühmann, K.; Müller, M.; Kölln, K.; Hamilton, M.; Burghammer, M.; Roth, S. V.; Stanzl-Tschegg, S.; Fratzl, P. Cell-wall recovery after irreversible deformation of wood. *Nat. Mater.* **2003**, *2*, 810−813.
(22) Fratzl, P.; Burgert, I.; Gupta, H. S. On the role of interface polymers for the mechanics of natural polymeric composites. *Phys. Chem. Chem. Phys.* **2004**, *6*, 5575−5579.
(23) Klemm, D.; Kramer, F.; Moritz, S.; Lindström, T.; Ankerfors, M.; Gray, D.; Dorris, A. Nanocelluloses: a new family of nature-based materials. *Angew. Chem., Int. Ed.* **2011**, *50*, 5438−5466.
(24) Turbak, A. F.; Snyder, F. W.; Sandberg, K. R. Microfibrillated cellulose, a new cellulose product: properties, uses, and commercial potential. *J. Appl. Polym. Sci.: Appl. Polym. Symp.*; ITT Rayonier Inc., Shelton, WA, 1983; pp 815−827.
(25) Henriksson, M.; Henriksson, G.; Berglund, L.; Lindström, T. An environmentally friendly method for enzyme-assisted preparation of microfibrillated cellulose (MFC) nanofibers. *Eur. Polym. J.* **2007**, *43*, 3434−3441.
(26) Pääkkö, M.; Ankerfors, M.; Kosonen, H.; Nykänen, A.; Ahola, S.; Österberg, M.; Ruokolainen, J.; Laine, J.; Larsson, P. T.; Ikkala, O.; Lindstrom, T. Enzymatic hydrolysis combined with mechanical shearing and high-pressure homogenization for nanoscale cellulose fibrils and strong gels. *Biomacromolecules* **2007**, *8*, 1934−1941.
(27) Saito, T.; Nishiyama, Y.; Putaux, J.-L.; Vignon, M.; Isogai, A. Homogeneous suspensions of individualized microfibrils from TEMPO-catalyzed oxidation of native cellulose. *Biomacromolecules* **2006**, *7*, 1687−1691.
(28) Larsson, P. A.; Berglund, L. A.; Wågberg, L. Ductile all-cellulose nanocomposite films fabricated from core−shell structured cellulose nanofibrils. *Biomacromolecules* **2014**, *15*, 2218−2223.
(29) McKee, J. R.; Huokuna, J.; Martikainen, L.; Karesoja, M.; Nykänen, A.; Kontturi, E.; Tenhu, H.; Ruokolainen, J.; Ikkala, O. Molecular engineering of fracture energy dissipating sacrificial bonds into cellulose nanocrystal nanocomposites. *Angew. Chem., Int. Ed.* **2014**, *126*, 5149−5153.
(30) Hoy, R. S.; Robbins, M. O. Strain hardening of polymer glasses: effect of entanglement density, temperature, and rate. *J. Polym. Sci., Part B: Polym. Phys.* **2006**, *44*, 3487−3500.
(31) Hoy, R. S.; O'Hern, C. S. Viscoplasticity and large-scale chain relaxation in glassy-polymeric strain hardening. *Phys. Rev. E* **2010**, *82*, 041803−1−041803−10.
(32) Solomon, M. J.; Spicer, P. T. Microstructural regimes of colloidal rod suspensions, gels, and glasses. *Soft Matter* **2010**, *6*, 1391−1400.
(33) Linder, M. B.; Qiao, M.; Laumen, F.; Selber, K.; Hyytiä, T.; Nakari-Setälä, T.; Penttilä, M. E. Efficient purification of recombinant proteins using hydrophobins as tags in surfactant-based two-phase systems. *Biochemistry* **2004**, *43*, 11873−11882.
(34) Nakari-Setälä, T.; Aro, N.; Kalkkinen, N.; Alatalo, E.; Penttilä, M. Genetic and biochemical characterization of the *Trichoderma reesei* hydrophobin HFBI. *Eur. J. Biochem.* **1996**, *235*, 248−255.
(35) Linder, M.; Salovuori, I.; Ruohonen, L.; Teeri, T. T. Characterization of a double cellulose-binding domain synergistic high affinity binding to crystalline cellulose. *J. Biol. Chem.* **1996**, *271*, 21268−21272.
(36) Varjonen, S.; Laaksonen, P.; Paananen, A.; Valo, H.; Hähl, H.; Laaksonen, T.; Linder, M. B. Self-assembly of cellulose nanofibrils by genetically engineered fusion proteins. *Soft Matter* **2011**, *7*, 2402−2411.
(37) Laaksonen, P.; Kainlauri, M.; Laaksonen, T.; Shchepetov, A.; Jiang, H.; Ahopelto, J.; Linder, M. B. Interfacial engineering by proteins: exfoliation and functionalization of graphene by hydrophobins. *Angew. Chem., Int. Ed.* **2010**, *49*, 4946−4949.
(38) Laaksonen, P.; Walther, A.; Malho, J. M.; Kainlauri, M.; Ikkala, O.; Linder, M. B. Genetic engineering of biomimetic nanocomposites: diblock proteins, graphene, and nanofibrillated cellulose. *Angew. Chem., Int. Ed.* **2011**, *50*, 8688−8691.
(39) Johnson, M.; Walter, S.; Flinn, B.; Mayer, G. Influence of moisture on the mechanical behavior of a natural composite. *Acta Biomater.* **2010**, *6*, 2181−2188.
(40) Teeri, T.; Salovuori, I.; Knowles, J. The molecular cloning of the major cellulase gene from *Trichoderma reesei*. *Nat. Biotechnol.* **1983**, *1*, 696−699.
(41) Teeri, T. T.; Lehtovaara, P.; Kauppinen, S.; Salovuori, I.; Knowles, J. Homologous domains in *Trichoderma reesei* cellulolytic enzymes: gene sequence and expression of cellobiohydrolase II. *Gene* **1987**, *51*, 43−52.
(42) Burgert, I.; Frühmann, K.; Keckes, J.; Fratzl, P.; Stanzl-Tschegg, S. E. Microtensile testing of wood fibers combined with video extensometry for efficient strain detection. *Holzforschung* **2003**, *57*, 661−664.
(43) Barth, A. Infrared spectroscopy of proteins. *Biochim. Biophys. Acta, Bioenerg.* **2007**, *1767*, 1073−1101.
(44) Jean-Louis Barrat, J. B.; Lyulin, A. Molecular dynamics simulations of glassy polymers. *arXiv* **2010**, 1002.2065.

Supporting Information

Enhanced Plastic Deformations of Nanofibrillated Cellulose Film by Adsorbed Moisture and Protein Mediated Interactions

Jani-Markus Malho, Claudiane Ouellet-Plamondon, Markus Rüggeberg, Päivi Laaksonen, Olli Ikkala, Ingo Burgert and Markus B. Linder

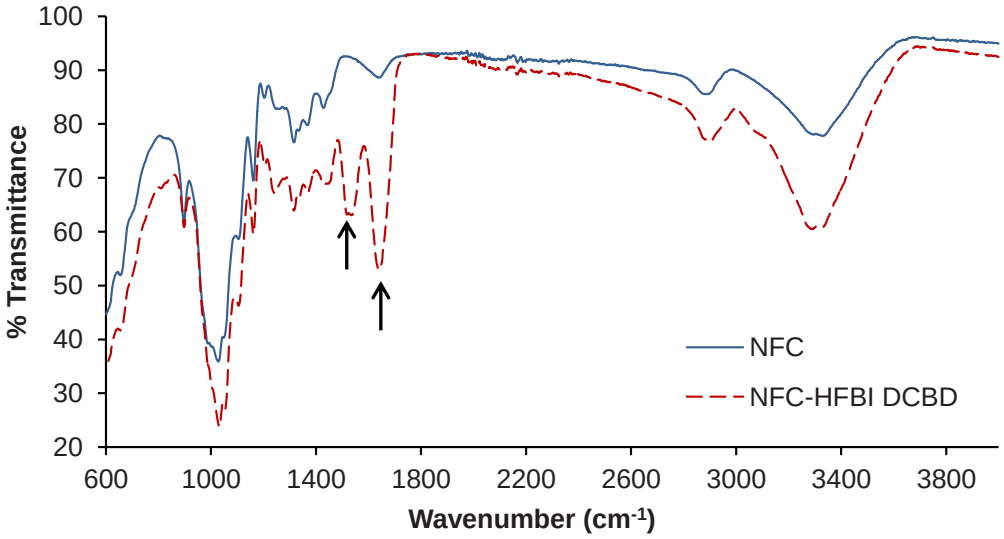

Figure S1. FTIR measurements of the unmodified NFC film and the NFC/DCBD-HFBI hybrid film. The arrows show Amide I band at 1639 cm^{-1} associated with the C=O vibration in antiparallel beta-sheets and an Amide II band at 1518 cm^{-1} associated with the N-H bending vibration and the C-N stretching vibration confirming the presence of the fusion protein in the modified NFC film.

TGA measurements were performed on NFC films, NFC/DCBD-HFBI films and the DCBD-HFBI protein alone (figure S2). Three maxima are visible in the derivative thermogravimetric (DTG) curves. The first maximum below 100°C corresponds to the evaporation of the adsorbed water. The evaporation of the adsorbed water was 3.3% for the NFC, 5.3% for the NFC-Protein and 6% for the pure DCBD-HFBI (Table 1). The higher amount of evaporated water for the NFC-DCBD-HFBI

film confirms the results of the DVS that the water content of the NFC/DCBD-HFBI film is higher than that of the unmodified NFC film at a certain relative humidity. The protein shows a second maximum at 300°C corresponding to its degradation. Both films show a second maximum at 350°C corresponding to the depolymerization, dehydration and decomposition of the glycosyl units. Hereby, the sample with the protein shows a shoulder at 300°C, which corresponds to the degradation of the fusion protein. The third maximum corresponds to the formation of charred residue and is more apparent in the protein sample. The third DTG maximum at 410-420°C was caused by oxidation and breakdown of the char to gaseous product.

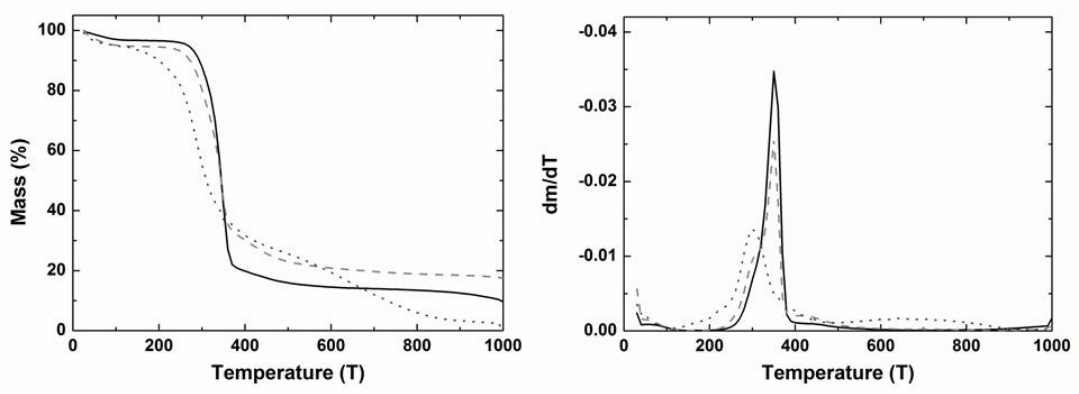

Figure S2. Thermogravimetric (left) and derivative thermogravimetric (DTG) curves (right) of unmodified NFC film, NFC/DCBD-HFBI film and pure DCBD-HFBI protein (Black solid line, light grey dashed line and dark grey dotted line, respectively).

Table 1. Mass loss of the TGA.

T (°C)	NFC	NFC/DCBD-HFBI	HFBI DCBD
25 - 150	3.3%	5.3%	6.0%
150 - 400	76.8%	64.5%	61.2%
400 - 600	5.3%	9.3%	12.7%
600 - 1000	5.0%	3.5%	18%
Residue	9.6%	17.4%	2%

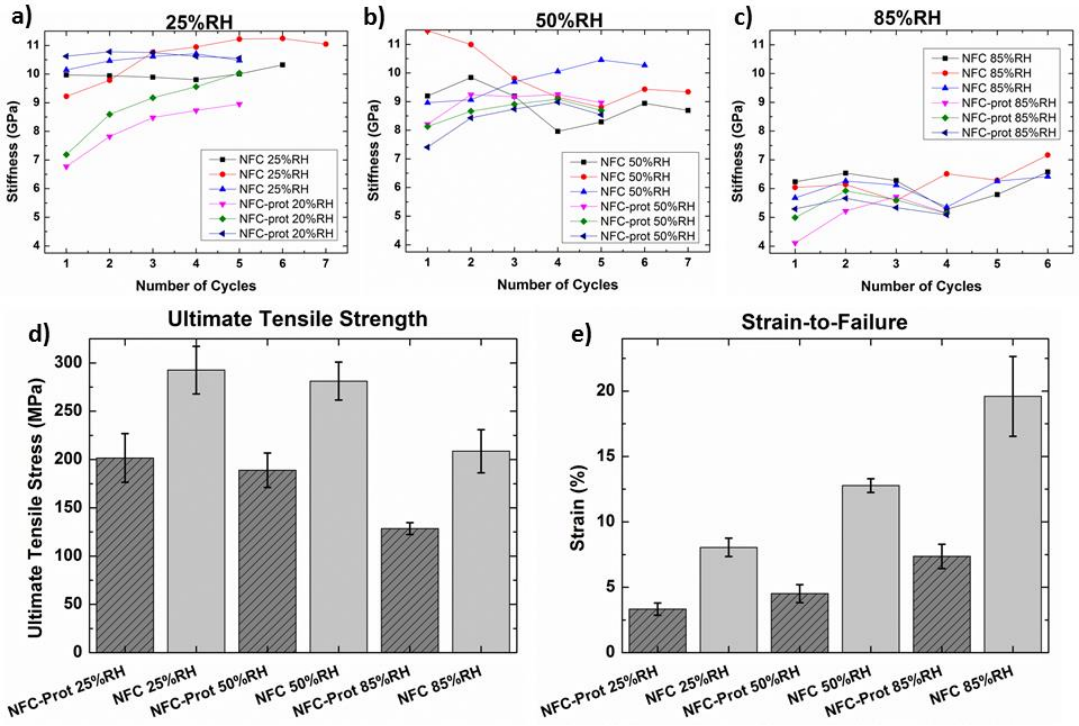

Figure S3. Cyclic measurements of unmodified NFC film and NFC/DCBD-HFBI hybrid films in 25%RH, 50%RH and 85%RH. a-c) Show three diagrams, where the development of stiffness during the cyclic measurements at 25%RH, 50%RH and 85%RH (a-c respectively) is drawn as a function of the cycles. d) Displays the average tensile strength for NFC/DCBD-HFBI and unmodified NFC films with standard deviation. e) Shows the average strain-at-failure values for NFC/DCBD-HFBI and NFC films with standard deviation.

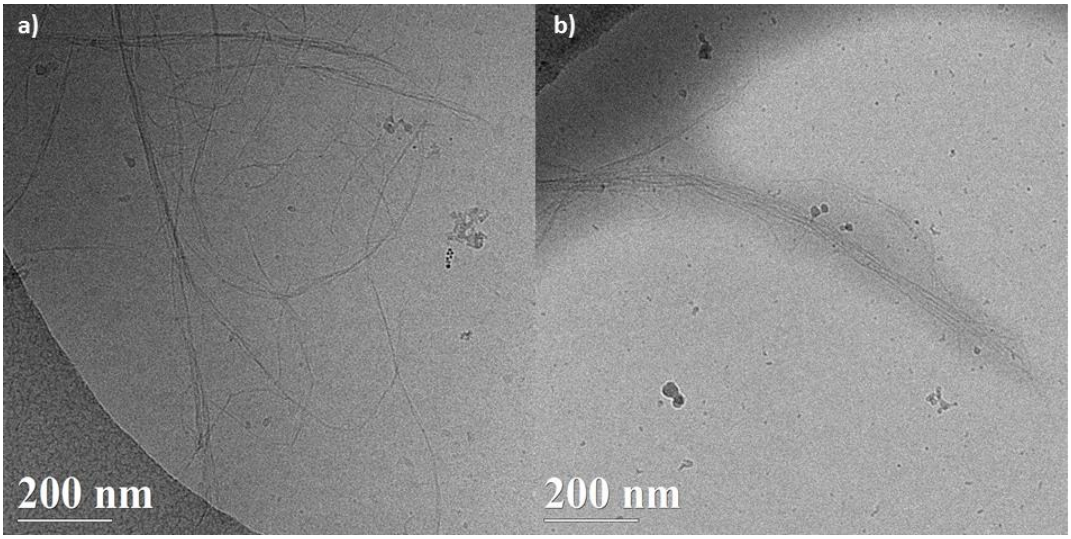

Figure S4. Cryo-TEM images of vitrified dispersions of a) unmodified NFC nanofibers and b) HFBI-DCBD modified NFC nanofiber dispersion.